Evolution of Catalytic Activity of Au−Ag Bimetallic Nanoparticles on Mesoporous Support for CO Oxidation

Ai-Qin Wang,[†] Chun-Ming Chang,[‡] and Chung-Yuan Mou*[,†]

Department of Chemistry, National Taiwan University, Taipei 106, Taiwan, and Department of Physics, National Dong Hwa University, Hualien 974, Taiwan

Received: March 24, 2005; In Final Form: August 5, 2005

We report a novel Au−Ag alloy catalyst supported on mesoporous aluminosilicate Au−Ag@MCM prepared by a one-pot synthesis procedure, which is very active for low-temperature CO oxidation. The activity was highly dependent on the hydrogen pretreatment conditions. Reduction at 550−650 °C led to high activity at room temperature, whereas as-synthesized or calcined samples did not show any activity at the same temperature. Using various characterization techniques, such as XRD, UV−vis, XPS, and EXAFS, we elucidated the structure and surface composition change during calcination and the reduction process. The XRD patterns show that particle size increased only during the calcination process on those Ag-containing samples. XPS and EXAFS data demonstrate that calcination led to complete phase segregation of the Au−Ag alloy and the catalyst surface is greatly enriched with AgBr after the calcination process. However, subsequent reduction treatment removed Br^- completely and the Au−Ag alloy was formed again. The surface composition of the reduced Au−Ag@MCM (nominal Au/Ag = 3/1) was more enriched with Ag, with the surface Au/Ag ratio being 0.75. ESR spectra show that superoxides are formed on the surface of the catalyst and its intensity change correlates well with the trend of catalytic activity. A DFT calculation shows that CO and O_2 coadsorption on neighboring sites on the Au−Ag alloy was stronger than that on either Au or Ag. The strong synergism in the coadsorption of CO and O_2 on the Au−Ag nanoparticle can thus explain the observed synergetic effect in catalysis.

Introduction

Since Haruta's initial report[1] on the exceptionally high activity of supported gold catalysts, extensive research work both in fundamental and in application has been carried out in order to understand the origin of the surprisingly active catalytic behavior of the gold nanoparticle.[2−10] It has been established that the catalytic performance of the gold nanoparticle is sensitive to the particle size, the support, and the preparation procedure. In principle, such size and support dependence is related to the adsorption of reactants, especially to the activation of oxygen. Because gold does not adsorb oxygen well, the choice of support becomes important so that it can provide reactive oxygen. In the case of inert support, the particle size of gold has to be critically controlled in the range of 2−3 nm so both oxygen and carbon monoxide are thus adsorbed and activated on the gold surface.[11]

One way to obtain an active gold catalyst on an inert support is to make nanoparticles of gold alloy with a second metal that plays the role of activating oxygen.[12,13] In a previous letter,[14] we reported a catalyst system of Au−Ag alloy nanoparticles supported on mesoporous aluminosilicate showing exceptionally high activity of CO oxidation, comparable to the most active catalyst, Au/TiO_2. It was found that a synergistic effect exists between Au and Ag, leading to higher activity than either pure metallic catalyst.[14] For the alloy catalyst, the average particle size is rather large, 20−30 nm. In this alloy system, the size effect is no longer a critical factor, whereas Ag is believed to play a key role in the activation of oxygen. Further detailed research is needed to understand the origin of this exceptionally catalytic behavior.

There are at least three important factors affecting the catalytic property of the Au−Ag alloy: the chemical composition (Au/Ag ratio), the Al content in the support, and the pretreatment conditions for activating the catalyst. In this paper, we would like to focus on the effect of calcination and reduction treatment on the structure change and thereby on the catalytic properties of the Au−Ag alloy.

For a supported gold catalyst, pretreatment plays an important role in evolving high activity and the effect differs greatly between catalyst systems. For Au/TiO_2 prepared by deposition-precipitation, calcination at 300 °C often results in high activity.[15] This has been attributed to the formation of metallic gold with smaller particle size. However, for the Au/TiO_2 catalyst prepared by grafting the $[Au_6(PPh_3)_6](BF_4)_2$ complex onto TiO_2, a combination of high-temperature reduction and then low-temperature oxidation resulted in a very active CO oxidation catalyst.[16] However, for the Au/Fe_2O_3 catalyst system,[17] the as-synthesized samples exhibited higher activity than the calcined samples. For Au/Al_2O_3, the pretreatment has a more complex effect.[18,19] Costello et al.[20] investigated the effect of pretreatment temperature and atmosphere on the structure and activity of Au/Al_2O_3 in detail. They found that pretreatment of Au/Al_2O_3 with a mixture of H_2 and O_2 or H_2O at 100 °C led to the highest CO conversion, implying that water or surface species derived from water plays a significant role.

In our bimetallic catalyst system, the pretreatment effect becomes more complex because the gas environment during pretreatment may affect the preferential surface segregation of

* Corresponding author. E-mail: cymou@ntu.edu.tw. Fax: +886-2-2366-0954.
[†] National Taiwan University.
[‡] National Dong Hwa University.

10.1021/jp051530q CCC: $30.25
Published on Web 09/15/2005

one of the two metals.[21−23] In the present work, we study the changes in structure and composition of Au−Ag bimetallic catalysts, under various activation procedures, using XRD, XPS, and EXAFS techniques and correlating the structure changes with their catalytic activities.

For the reaction mechanism, we proposed previously that Ag plays a key role in the activation of oxygen.[14] Most likely, the CO oxidation reaction occurred on the neighboring sites above Au and Ag atoms where Au adsorbs CO and Ag adsorbs O_2. In this work, we perform an EPR (electron paramagnetic resonance) study of the catalysts to look for the activated species superoxide O_2^- species in them. EPR is a very sensitive technique for the detection of O_2^- formation on the catalyst surface. For supported Au nanocatalysts, there have been recent EPR studies[24,25] indicating that the adsorbed species O_2^- is involved in the oxidation of CO. The extra electron on the adsorbed superoxide could be a result of electron transfer from the AuAg alloy.

Finally, a density functional theory (DFT) calculation shows that the coadsorption of CO and O_2 on neighboring Au and Ag atoms is indeed synergistic, leading to a larger adsorption energy than that on the Au nanoparticle.

Experimental Section

Catalyst Preparation. The Au−Ag alloy nanoparticles deposited on mesoporous aluminosilicate support (denoted as Au−Ag@MCM) were synthesized in a one-pot approach.[14,26] Briefly, a proper amount of $HAuCl_4$ (Aldrich) and $AgNO_3$ (Acros) was added into an aqueous solution of quaternary ammonium surfactant CTAB (Acros) to form a clear yellow-colored solution. Then, $NaBH_4$ solution was added and a dark-red solution was formed. After that, the Au−Ag alloy nanoparticle solution was poured directly into a sodium aluminosilicate solution and a red-colored precipitate formed immediately. The gel solution was then transferred to an autoclave to undergo hydrothermal reaction at 100 °C for 6 h. Overall, the molar ratio in the aluminosilicate gel is 1.0 SiO_2/0.042 $NaAlO_2$/0.18 CTAB/493 H_2O, and the total metal loading was 8 wt %. Otherwise mentioned, the Au/Ag molar ratios mentioned below are nominal values, and they are consistent with the analytical results by EDX.

Catalyst Characterization. The UV−vis spectra were recorded on the Hitachi U-3010 UV−vis spectrophotometer at ambient temperature operating in the reflection mode at a resolution of 2 nm using barium sulfate as a standard for the background correction.

The powder X-ray diffraction patterns (XRD) were collected on a Philips PW 1830 instrument operating at 45 kV voltage and a current of 40 mA with Cu Kα radiation in the 2θ range from 20° to 80°.

XPS spectra were obtained with a VG ESCALAB 250 equipped with a monochromated Al Kα radiation source (1486.6 eV) under a residual pressure of 10^{-9} Torr. For charge compensation, a flood gun with variable electronvoltage (from 6 to 8 eV) was used. The raw data were corrected for substrate charging using the binding energy of the Si-2p peak (103.3 eV) on aluminosilicate support as references. The measured spectra were fit by a least-squares procedure to a product of Gaussian−Lorentzian functions after subtraction of background noise. The concentration of each element was calculated from the area of the corresponding peak, calibrated using the sensitivity factor of Wagner.

Electron paramagnetic resonance (EPR) spectra were recorded at 84 K with a Brüker EMX spectrometer working in the X-band (9.53 GHz). A weighted catalyst of 20 mg was placed inside a 4-mm o.d. quartz tube with greaseless stopcocks. Prior to each measurement, the catalysts were first exposed to air, and then evacuated at room temperature until the residual pressure was below 1×10^{-3} Torr.

The extended X-ray absorption fine structure (EXAFS) spectra were recorded at the Beam Line 17C and 01C at the National Synchrotron Radiation Research Center (NSRRC), Hsinchu, Taiwan. The electron storage ring was operated at 1.5 GeV with a beam current of 100−200 mA. Both the Au L_{III}-edge and Ag K-edge absorbance of powder catalysts were measured in transmission geometry. The EXAFS data analysis was carried out using the UWXAFS package.

Catalytic Activity for CO Oxidation. The CO oxidation reaction was performed in a continuous flow fixed-bed microreactor. A catalyst (0.04 g) was used in each experiment. Prior to measurement, the catalyst was prereduced in situ under 10% H_2 in N_2 at 600 °C for 1 h. The reactant gases were purified by 4-Å molecular sieves and then mixed and passed into the reactor. The water vapor content in the reactant stream is no more than 4 ppm. The reactant flow consisted of a mixture of 1% CO and 4% O_2 with He as the balance. A total gas flow of 66.7 mL min^{-1} was applied corresponding to a GHSV of about 100 000 mL g_{cat}^{-1} h^{-1}. The reactants and products were analyzed online with a HP6890 gas chromatograph equipped with a Carboxen1000 column and TCD detector. The CO conversion is defined as the amount of CO_2 produced divided by the total amount of CO fed to the catalyst.

Computational Study

To understand the synergistic effect between Au and Ag, we calculated the adsorption energy of O_2 and CO on the monometallic and alloy Au−Ag particles using DFT (density functional theory).[27] The calculation was performed using the Vienna Ab initio Simulation Package (VASP)[28] with the projector-augmented wave (PAW) method.[29] The plane-wave basis is expanded with the kinetic energy cutoff of 400 eV. For the exchange-correlation functional, we used the spin-polarized generalized gradient approximation (GGA) as reported by Perdew et al.[30] The geometry of the cluster with or without adsorbate is fully optimized until the total energy is converged to 10^{-6} eV in the self-consistent loop and the force on each atom is less than 0.01 eV/Å. The 55-atom clusters are modeled with the icosahedral structure, which is the most stable structure among the high-symmetry arrangements such as the icosahedral, cuboctahedral, and decahedral structures for Au_{55} and Ag_{55} clusters in our calculations.

Results

In this section, we first present the effects of the reduction treatment of the catalyst on its catalytic activities and structures. We then show the results of spectroscopic characterization and theoretical calculations to pinpoint the reaction sites on the catalyst.

Effect of Reduction Temperature. In our previous report,[14] it was found that the Au−Ag alloy nanocatayst with a composition of Au/Ag of 3/1 gives the highest activity. In this work, we therefore fix the metal composition at this ratio and study the origin of its unusual activity in CO oxidation. Figure 1 shows the CO conversion over Au−Ag@MCM (Au/Ag = 3/1) reduced at various temperatures. It can be seen that the temperature of hydrogen treatment has a significant effect on the catalytic activity of Au−Ag@MCM. A reduction treatment between 550 and 600 °C led to the highest activity; CO can be

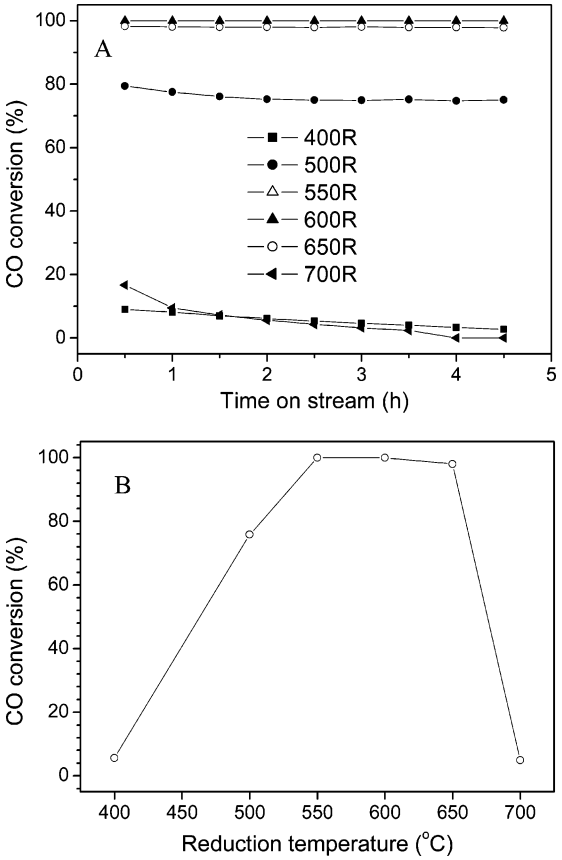

Figure 1. (A) CO conversion versus time-on-stream; (B) CO conversion versus the reduction temperature. Catalyst: Au−Ag@MCM with Au/Ag ratio of 3/1. The reaction was conducted at room temperature with space velocity of 100 000 mL/g_{cat} h.

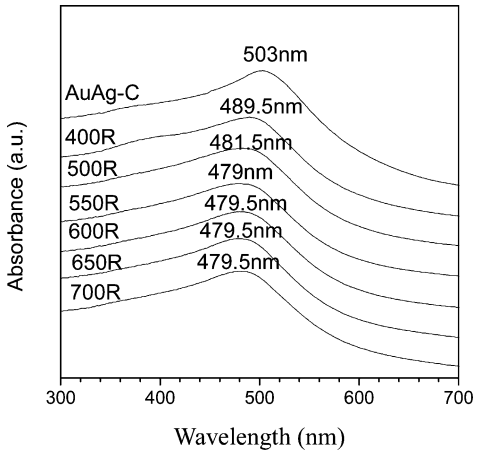

Figure 2. UV−vis spectra of catalysts reduced at different temperatures.

converted completely at room temperature. However, the catalysts reduced at either 400 or 700 °C exhibited lower activity; room-temperature CO conversion is below 10%. The order of activity with the reduction temperature is as follows: 550R ≈ 600R > 650R > 500R > 700R ≈ 400R (the number here denotes the reduction temperature in Celsius).

Figure 2 shows the UV−vis spectra of the catalysts reduced at various temperatures. The reduction pretreatment caused a large blue shift of the absorption bands. For example, the calcined sample has an absorption band at 503 nm, which blue-shifted to 489.5 nm after reduction at 400 °C. With a further increase of reduction temperature to 500 °C and higher, the maxima of the absorption band moved to shorter wavelength

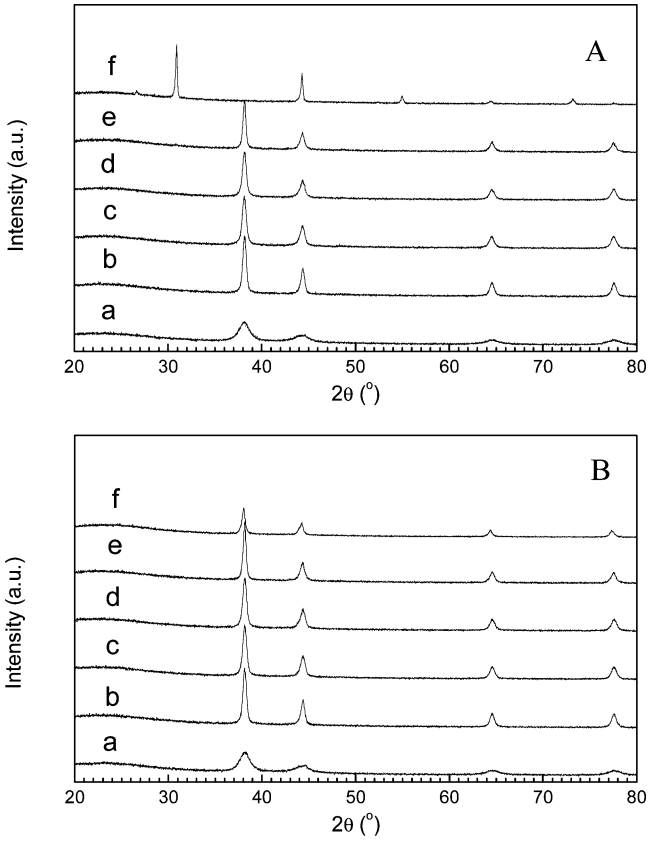

Figure 3. Wide-angle XRD patterns of calcined (A) and reduced (B) samples with different nominal Au/Ag ratios (a) Au/Ag = 1/0; (b) Au/Ag = 8/1; (c) Au/Ag = 5/1; (d) Au/Ag = 3/1; (e) Au/Ag = 1/1; (f) Au/Ag = 0/1.

until it stabilized at 479 nm. Because the position of the maximum absorption band of the Au−Ag alloy is related to the surface structure and composition,[31,32] the blue-shift of the SPR band with the higher reduction temperature implied either structure or surface composition changes with high-temperature reduction.

Structure Change during Calcination and Reduction Treatment. For the bimetallic catalysts, pretreatment may not only cause changes in surface composition but also bring about structure change. Figure 3 shows the XRD patterns of the calcined and reduced samples with various Au/Ag ratios. From Figure 3A, one can see that all of the bimetallic samples have the same XRD patterns as those of the monometallic Au@MCM sample, characterized by the four peaks positioned at 2θ = 38.2°, 44.3°, 64.5°, and 77.6°. These four peaks correspond to the (111), (200), (220), and (311) lattice planes,[33] respectively. Because gold and silver have almost the same lattice constant (0.408 nm versus 0.409 nm), the XRD pattern cannot distinguish between alloy and pure metals. In contrast to Au@MCM and Au−Ag@MCM samples, the calcined Ag@MCM shows a completely different XRD pattern, which is assigned to the AgBr phase. Inferred from the XRD pattern of Ag@MCM, we believe that the calcined bimetallic catalyst may include some AgBr. However, it may be below the XRD detection limit because of the low concentration of Ag in the bimetallic samples (for example, the Ag concentration was only 1.2 wt % when Au/Ag = 3/1).

The bromide in AgBr comes from the surfactant CTAB. However, after the samples were reduced, they exhibited the same XRD patterns as that of Au@MCM (Figure 3B), no matter what the Au/Ag ratio was. This indicates that the reduction treatment removed the Br^- species completely and alloys are

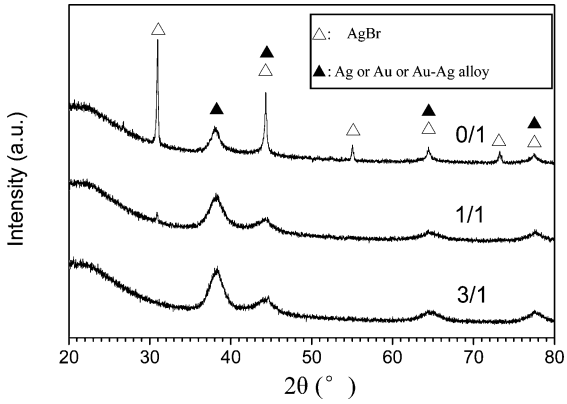

Figure 4. Wide-angle XRD patterns of as-synthesized Au−Ag@MCM with different Ag contents.

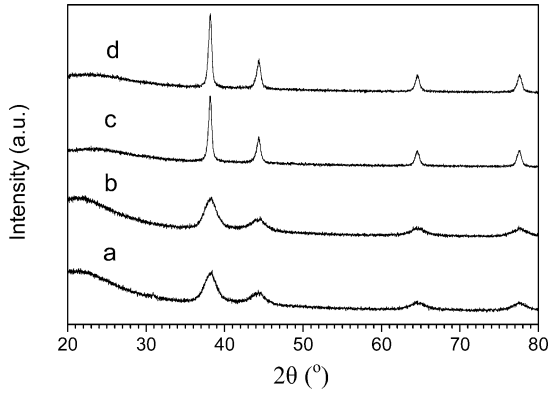

Figure 5. Wide-angle XRD patterns of Au−Ag@MCM with Au/Ag = 3/1 (a) as-synthesized; (b) after hydrothermal treatment at 100 °C for 6 h; (c) after calcined at 560 °C for 6 h; (d) after reduction at 600 °C for 1 h.

formed again. In fact, our elemental analysis results show that Br^- was not detected after the sample was reduced.[34]

To understand the AgBr formation that occurred during the preparation of the catalysts, we conducted the XRD measurements on the as-synthesized samples of variated Au/Ag ratios. As shown in Figure 4, on the sample Ag@MCM, the XRD peaks corresponding to AgBr phase (sharp peak) and Ag phase (broad peak) were observed. For comparison, on the Au−Ag@MCM with Au/Ag ratio of 1/1, only a very small AgBr peak was observed, accompanied by the four broad Au or Au−Ag alloy peaks. With a further decrease of Ag content (Au/Ag = 3/1), only the Au or Au−Ag alloy phase was detected. This result indicates that the AgBr phase already exists on the as-synthesized Ag-containing samples. We notice that upon addition of $AgNO_3$ to the CTAB solution when we prepared the Ag@MCM, a white precipitate formed immediately, indicating formation of AgBr. However, after the reducing agent $NaBH_4$ was added, the white precipitate disappeared gradually, and the solution became clear with a greenish-yellow color, implying AgBr had been reduced to nanoparticles of Ag. The maximum absorbance at ~400 nm confirmed the formation of Ag nanoparticles at this stage.[14] However, after mixing the above CTAB-protected Ag colloid with aluminosilicate solution, the gel formed was stirred for several hours. Considering that the Ag nanoparticle is not very stable (for example, after stirring for several hours, the clear solution of Ag colloid will become opaque and some precipitate will be formed again.), the formation of the AgBr phase, we guess, probably occurred during stirring of the gel. It should be pointed out that only a part of Ag reacted with Br^- to revert back to AgBr, and a substantial amount of metallic Ag or Au−Ag alloy existed on the as-synthesized samples.

Following that, the as-synthesized samples underwent hydrothermal treatment and calcination. As shown in Figure 5, the as-synthesized Au−Ag@MCM (Au/Ag = 3/1) sample shows rather broad XRD peaks, even after hydrothermal treatment, indicating that a rather small particle size was obtained (about 6−7 nm estimated from Scherrer's equation). However, after calcination, the XRD peaks become pretty sharp (the estimated particle size is about 20−30 nm), implying that severe aggregation and sintering occurred during the calcination. Further reduction treatment probably did not cause much sintering or aggregation, showing the same XRD peak width. However, comparing Figure 4 with Figure 3A, one can see that no metallic Ag was detected on the calcined Ag@MCM, indicating that calcination further facilitated the reaction between Ag and Br^-, causing complete conversion of metallic Ag to AgBr. Correspondingly, for the Au−Ag alloy phase, a complete phase segregation occurred during calcination, leading to the formation of Au and AgBr.

The changes that occurred during calcination and reduction are also confirmed by XPS investigation. As listed in Table 1, one can see that the binding energies of Au_{4f} have only a slight shift after reduction. However, comparing the Ag_{3d} binding energies of the calcined samples and the reduced samples, it is evident that the binding energy increase of Ag_{3d} is more than 1.0 eV. For example, for the sample with Au/Ag of 3/1, the binding energy of $Ag_{3d5/2}$ shifted from 366.5 to 368.0 eV after reduction, indicating the Ag(I) state for the calcined sample and metallic Ag after the reduction procedure. In contrast, the binding energy of $Au_{4f7/2}$ changed only slightly from 83.9 to 83.6 eV after reduction, implying gold is in the metallic state before and after reduction. This may be due to the preferential reaction between Br^- and Ag, compared with Au.

Moreover, from Table 1, one can see that the surface composition changed a little after reduction treatment. For the calcined Au−Ag@MCM bimetallic samples, the surface was greatly enriched with Ag. For example, when the Au/Ag ratio is 3/1, the surface Au/Ag decreased to 0.60 after calcination, implying that calcination not only caused aggregation of metal particles but also resulted in complete phase segregation, thus leading to the formation of the AgBr phase and enrichment of this phase to the surface. Compared to the original Au/Ag = 3/1 composition, the surface became more enriched with Ag and the surface Au/Ag ratio changed to 0.75 after reduction.

From the UV−vis spectra in Figure 2, one can see that the reduction treatment led to the blue-shift of the maximum

TABLE 1: XPS Analysis Results before and after Reduction Treatment

	before reduction					after reduction				
Au/Ag (nominal value)	$Au_{4f7/2}$ (eV)	$Au_{4f5/2}$ (eV)	$Ag_{3d5/2}$ (eV)	$Ag_{3d3/2}$ (eV)	Au/Ag (atomic)	$Au_{4f7/2}$ (eV)	$Au_{4f5/2}$ (eV)	$Ag_{3d5/2}$ (eV)	$Ag_{3d3/2}$ (eV)	Au/Ag (atomic)
1/0	83.7	87.4				83.4	87.1			
3/1	83.9	87.6	366.5	372.5	0.60	83.6	87.3	368.0	374.0	0.75
1/1	84.0	87.7	367.2	373.2	0.29	83.8	87.5	368.2	374.2	0.43
0/1			366.9	372.7				368.5	374.5	

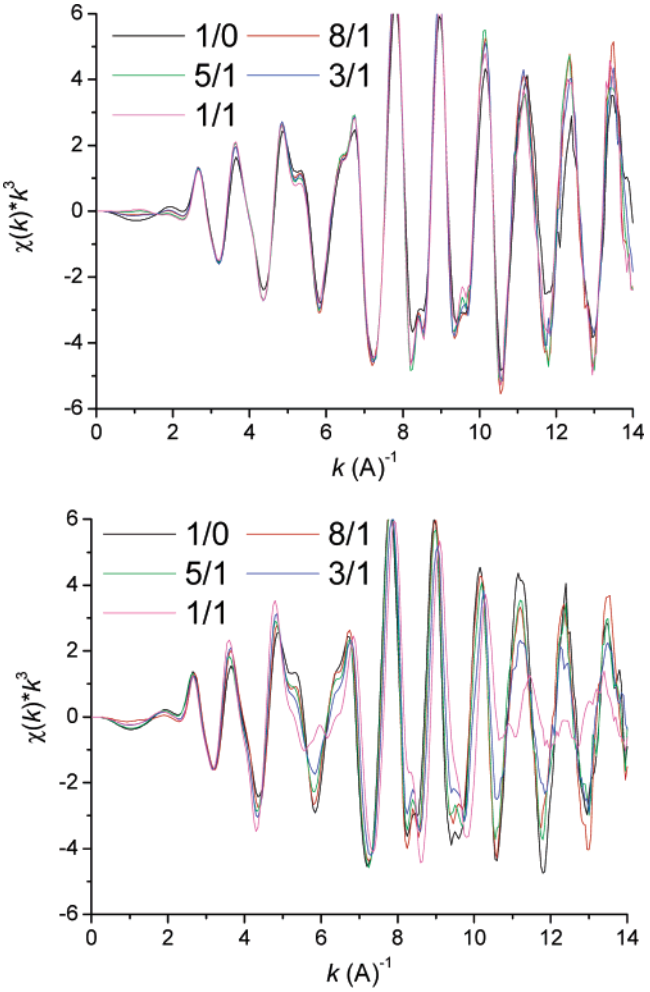

Figure 6. Au L_3 edge EXAFS oscillations, k^3-weighted Chi function of the calcined (top) and reduced (bottom) samples with different Au/Ag ratios.

absorption band. In the case of the Au−Ag alloy, such a blue-shift seems to imply a decrease of the Au/Ag ratio. XPS results also indicate a decrease of the Au/Ag ratio (Table 1). Because extended X-ray absorption fine structure spectroscopy (EXAFS) has proven to be powerful in identifying the occupation of sites around specific atoms, we use the EXAFS technique to determine the structure change during the reduction process.

Figure 6 shows the Au L_3 edge EXAFS spectra ($\chi(k^3)$) of the calcined and reduced samples with various Au/Ag ratios, and Figure 7 shows the corresponding Fourier transform of $\chi(k^3)$ where the range $k = 3-11$ Å^{-1} is transformed. Clearly, for the calcined samples, no matter what the Au/Ag ratio is, the EXAFS spectra are almost the same as Au@MCM, suggesting that the nearest neighboring atom to Au is not Ag, but Au. In other words, in calcined samples, Au and Ag did not form an alloy but existed as separate phases, AgBr and metallic gold, as indicated by the XRD and XPS results. However, after reduction, the oscillatory features at approximately $k = 6$ Å^{-1} changed greatly with the increase of Ag concentration. This results from the increase of the Ag nearest neighbors around Au atoms because Au and Ag have quite different backscattering phase shifts at higher k. However, from the r-space radial distribution of EXAFS, one can also see that with a decrease of the Au/Ag ratio of the reduced samples, the peak intensity at a larger distance increases relative to that of the peak at a smaller distance because of changes in interference between the Au and Ag oscillations. When the Au/Ag ratio

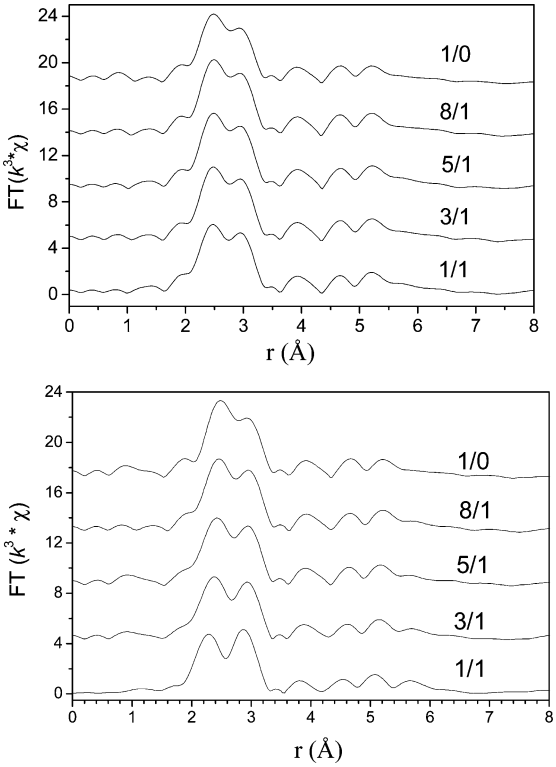

Figure 7. Au L_3 edge EXAFS, Fourier transform of $k^3\chi(k)$ for the calcined (top) and reduced (bottom) samples.

becomes 1/1, the two peaks have about the same intensities. In contrast, for the calcined samples, no matter what the Au/Ag ratio is, the intensity ratio of the two peaks is almost the same for all of the samples. It is worth noting that both peaks come from the first neighbor (with a single distance), but they appear at a shorter distance from the actual bond lengths because of the backscattering phase shift.

Ag K-edge EXAFS data of the reduced samples are shown in Figure 8. Evidently, with an increase of Ag concentration, both $\chi(k^3)$ oscillations and its Fourier transform spectra changed greatly, which is in good agreement with the above Au L_3-edge EXAFS data. However, unfortunately, when we investigate the Ag K-edge EXAFS spectra of the calcined samples, the signals are too weak to obtain good-quality oscillations. Anyway, the above EXAFS data clearly demonstrate that the reduction treatment not only removed the Br species attached to Ag and changed the surface composition but also led to the formation of the Au−Ag alloy.

From the above results, it can thus be concluded that the special calcination-reduction process is crucial for the formation of AuAg alloy nanoparticles with surface enrichment of Ag. The resulting nearly 1:1 Au/Ag surface ratio gives optimum catalytic activity. Very recently, Iizuka et al.[21] found that there is some impurity of silver in gold nanoparticles and the effect of the impurity is to enhance CO oxidation. The enhancement of surface silver content should make us cautious in interpreting many of the reported excellent catalytic activity of the Au nanocatalyst because the source gold materials may contain some silver as an impurity. The fact that the surface enrichment of Ag is sensitive to the pretreatment procedure may also be relevant in many of the studies of the gold catalyst.

Oxygen Adsorption. To provide direct evidence for the activation of reactive molecules, we conducted EPR measurements on the calcined and reduced samples as well as the sample after the oxidation reaction. The results of these air-exposed samples are shown in Figure 9. According to literature,[24,35] the

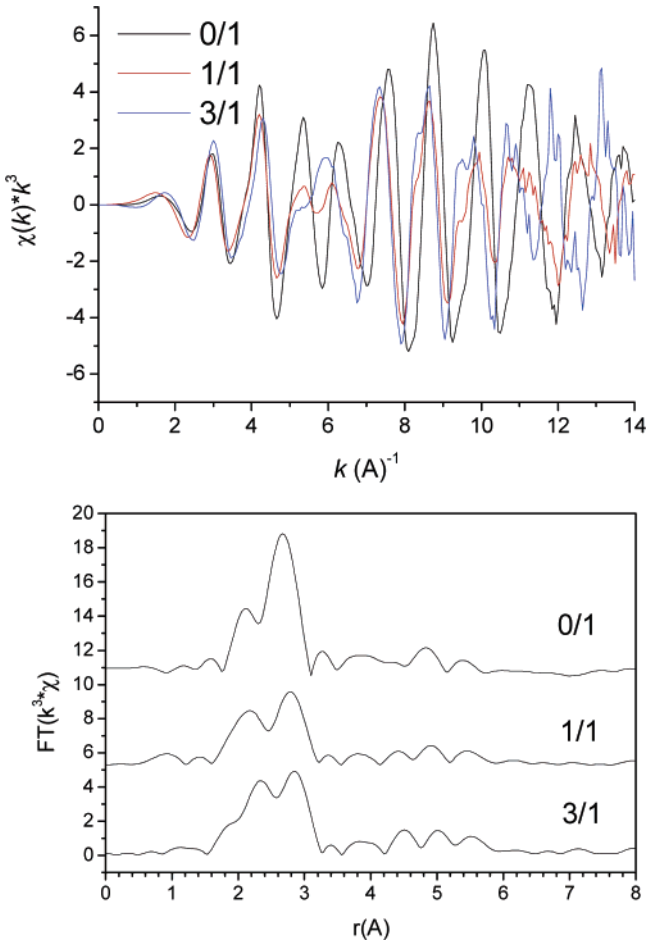

Figure 8. Ag K-edge EXAFS spectra of reduced samples with different nominal Au/Ag ratios. (top) k^3-weighted Chi function and (bottom) its Fourier transform.

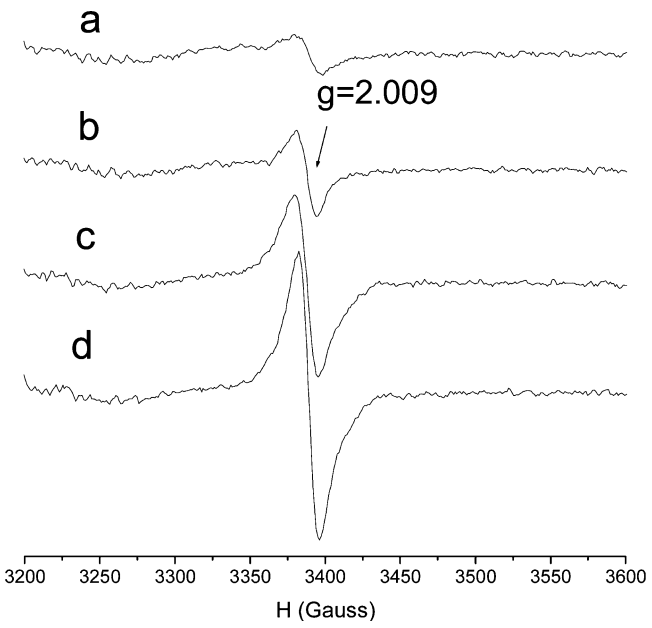

Figure 9. ESR spectra of (a) MCM-41 support; (b) calcined Au−Ag@MCM; (c) reduced Au−Ag@MCM; (d) Au−Ag@MCM after oxidation reaction. (Au/Ag = 3/1).

EPR signal at $g = 2.009$ can be assigned to the superoxide O_2^- formed on the catalyst surface. Clearly, with the reduction treatment, the intensity of O_2^- increased greatly. After the oxidation reaction test, the signal became even stronger. These results provide evidence that the reduction treatment increases the adsorption of oxygen after the formation of the Au−Ag alloy.

Discussion

We have demonstrated that the Au−Ag@MCM catalysts prepared by our unique one-pot synthesis procedure exhibited excellent catalytic activity for CO oxidation after a reduction treatment at 600 °C. In this synthesis procedure, the Au−Ag alloy was preformed in aqueous solution, evidenced by the SPR band in the UV−vis spectra.[14] However, after subsequent occluding into mesoporous material and high-temperature treatment, such as calcination and reduction, whether this Au−Ag alloy structure was retained or changed needs to be clarified. In this paper, we try to unveil such a structure change using various characterization techniques.

As illustrated in Figures 4 and 5, when the Au−Ag alloy nanoparticles preformed in aqueous solution, together with the surfactant CTAB, were occluded into mesoporous material, the particle size of the Au−Ag alloy remained essentially unchanged, even after a hydrothermal treatment at 100 °C for 6 h. This is understandable in consideration of the stabilizing role of the surfactant. However, partial phase segregation occurred at this stage, indicated by the coexistence of both the Ag (Au−Ag alloy for the bimetallic samples) and AgBr phase. However, after calcination at 560 °C, which is necessary for the removal of surfactant, both the structure and particle size of the Au−Ag alloy nanoparticles changed significantly. On one hand, the particle size increased from 6−7 nm to 20−30 nm, as estimated from XRD line-width. On the other hand, the reaction between Ag and Br^- was complete after calcination, indicated by the fact that only the AgBr phase was detected on the Ag@MCM sample. Such a reaction leads to phase segregation and a great enrichment of AgBr on the surface. This was supported by the XRD pattern in Figure 3 and the XPS data in Table 1. The XPS data of calcined samples reveal that Ag existed in the Ag(I) state, whereas Au is still in its metallic form. This is because Br^- combined preferentially with Ag. It is known that gold is the most electronegative metal and is difficult to react directly with other electronegative elements.[3] Alternatively, Ag is more reactive and can form stable AgBr. The formation of AgBr not only caused more severe phase segregation of the Au−Ag alloy during calcination but also induced an increase of the size of metal particles. Because the melting point of AgBr (mp 432 °C) is much lower than that of metallic Ag (mp 960.5 °C) or Au (1063 °C), the formation of the AgBr phase, we believe, helps induce the sintering to a greater extent. This may explain why we observed in Figure 3 that all of the Ag-containing samples have sharper XRD peaks than pure Au@MCM.

The catalytic activity test shows that the calcined samples, either monometallic or bimetallic, did not exhibit any catalytic activity for CO oxidation. It has been known that chloride is a poison for the gold catalyst in CO oxidation.[2,3] Inferred from this, bromide might act as a similar poison. Therefore, the reduction treatment prior to the activity test is necessary to remove the bromide completely. EXAFS measurements revealed that together with the bromide removal during reduction, the Au−Ag alloy was formed again. The activity test results shown in Figure 1 indicate that 550−650 °C is the optimum reduction temperature. Reduction at lower temperatures may be not enough to remove Br^- completely or not enough to form the Au−Ag alloy. Alternatively, a temperature of reduction that is too high may lead to further enlargement of the particles or may partially destroy the mesoporous structure. The blue shift

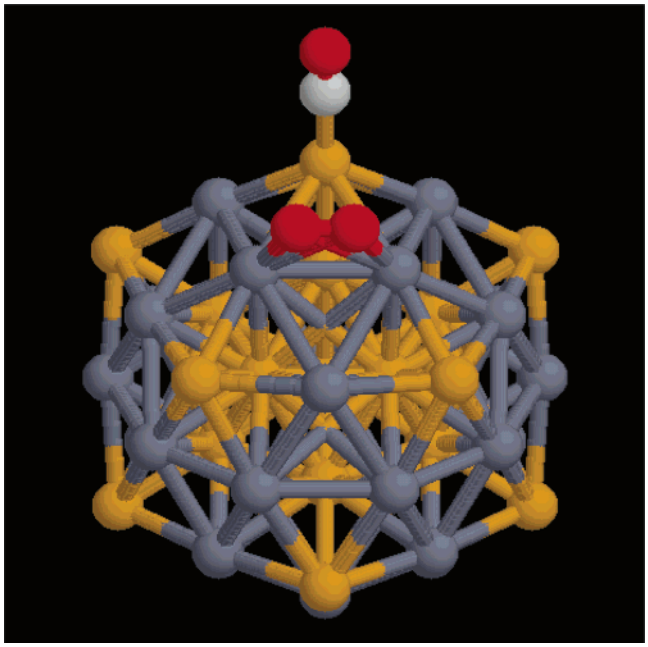

Figure 10. Structure model for CO and O_2 adsorption. The yellow balls on the surface represent Au atoms at the vertex sites of $Au_{25}Ag_{30}$ alloy nanoparticle. The blue balls represent Ag atoms at the edge sites of $Au_{25}Ag_{30}$ alloy nanoparticle. The red balls represent the oxygen atoms, and the gray ball is for the carbon atom.

in the UV−vis spectra with reduction in temperature as observed in Figure 2 may result from the phase change from a mixture of Au and AgBr to a complete Au−Ag alloy. In addition, the chemical composition of the catalyst surface changed slightly by the reduction treatment, and the surface Au/Ag ratio of the optimum catalyst (with nominal Au/Ag ratio being 3/1) is close to 1. According to our proposed mechanism,[14] alternatively intimate contact between Au and Ag would favor the synergism in activating O_2 and CO. The apparent optimum surface composition, close to 1, is thus understandable.

It is thus suggested that via alloying Au with Ag, the electronic properties of both Au and Ag were modified, resulting in a stronger tendency to lose electrons to the adsorbates. In CO oxidation, an electron transfer from the metal to the antibonding orbital of the O_2 molecule would help weaken the O−O bonding, thus improving the oxygen activation. Our EPR measurement indicates that by alloying Ag with Au (Figure 9c), the adsorption and activation of oxygen on the catalyst surface became stronger. Further coadsorption of a CO molecule makes the oxygen adsorption even stronger (Figure 9d). This inferred conclusion from EPR measurements is convincing but not conclusive. We thus perform a quantum chemical calculation to strengthen this view.

The Au and Ag monometallic particles were modeled with a 55-atom cluster in an icosahedral structure as shown in Figure 10. We have calculated the adsorption energies for CO and O_2 at various sites on the Au_{55} and Ag_{55} monometallic particles. For CO adsorption, the CO molecule preferred the "standing-up" configurations with carbon atom binding to the surface atom and the optimal adsorption site as the vertex site (Figure 10). The adsorption energy is −1.11 eV for Au_{55} and −0.44 eV for Ag_{55} (see Table 2). For O_2 adsorption, the O_2 molecule preferred the "lying-down" configurations with both oxygen atoms binding to the surface atoms. The most stable adsorption site is between these two configurations and aligned with the two edge atoms (see Figure 10); the adsorption energy for this configuration is −0.33 eV Au_{55} and −0.43 eV for Ag_{55}. From Table 2,

TABLE 2: Adsorption Energy of O_2 and CO Calculated by DFT According to the Model in Figure 10

	Ag_{55}	$Au_{25}Ag_{30}$	Au_{55}
E_{ads}(CO) (eV)	−0.44	−0.97	−1.11
E_{ads}(O_2) (eV)	−0.43	−0.58	−0.33
E_{ads}(CO + O_2) (eV)	−0.91	−1.55	−1.31

one can see that CO adsorbed on Au_{55} more strongly than on Ag_{55}, whereas the trend is the reverse for O_2 adsorption. This is in agreement with the literature reports.[36,37] Then, we construct a model alloy particle $Au_{25}Ag_{30}$, which contains 13 Au atoms in the core, 12 Au atoms on the surface vertex site (the optimal site for CO adsorption), and 30 Ag atoms on the surface edge site (the optimal site for O_2 adsorption) as shown in Figure 10.

For the Au−Ag alloy cluster, we constructed the ordered $Au_{25}Ag_{30}$ alloy cluster, which keeps the icosahedral structure for comparison with the monometallic clusters, and the atomic positions of Au and Ag atoms are arranged to have optimal adsorptions for both CO and O_2 as discussed. We have also done some calculations for disordered (here, the disorder means that the atomic positions of Au and Ag on the cluster surface is randomly mixed) $Au_{25}Ag_{30}$ bimetallic isocahedral clusters, and the ordered $Au_{25}Ag_{30}$ alloy cluster described in the text is more stable than the disordered ones that we have tested, which indicates it is at least a local minimum energy structure.

For the $Au_{25}Ag_{30}$ alloy particle, CO adsorption is weakened slightly, indicated by the slightly smaller adsorption energy (∼ −0.96 eV vs ∼ −1.11 eV) compared with CO on Au_{55}. However, the O_2 adsorption on $Au_{25}Ag_{30}$ is much stronger than that on either the Au_{55} or Ag_{55} monometallic particle. This is very important and helpful for the CO oxidation reaction. More importantly, when CO and O_2 molecules are coadsorbed on the nanoparticles, the total adsorption energy increased greatly in either the monometallic or alloy case. Because all of the 55-atom clusters (Au, Ag and Alloy) are modeled with the same (icosahedral) structure, the results clearly show the synergistic effect toward the activation of O_2 in the Au−Ag alloy nanocatalyst.

This result suggests that in the case of the Au−Ag alloy, CO and O_2 can be coadsorbed easily in the neighboring Au−Ag site. An electron transfer to the antibonding orbital of O_2 leads to the weakening of its bonding. This strong coadsorption and concomitant activation of oxygen would result in high reactivity in oxygen-atom transfer. In another words, the high catalytic activity of Au−Ag@MCM observed in our experiment can be attributed to the easy adsorption of O_2 on the Au−Ag alloy surface, which is formed only by the high-temperature reduction treatment. The fact that the intensity of the superoxide detected by EPR correlates rather well with reactivity further confirms this picture. Further computational studies that are in progress will give us a detailed molecular mechanism of the catalysis action of this novel Au−Ag alloy.

Finally, we discuss the role of the MCM-41 support. Because the metal particles are preformed in aqueous solution with a size of 6−7 nm, they are too big to be accommodated by the pore system of MCM-41 (the pore size of MCM-41 in our case is about 2.4 nm). Moreover, during calcination, the metal particles enlarged to 20−30 nm. TEM reveals that these particles are probably on the matrices of MCM-41 or just on the external surface of MCM-41.[14] However, it should be pointed out that in our one-pot synthesis procedure, the particle sizes of MCM-41 are less than 100 nm. There is a large amount of macropores formed by the agglomeration of nanosized MCM-41 particles. These macropores are in the size of 50−100 nm and can act as accommodations for Au−Ag alloy nanoparticles. Previously,

we have shown that reducing the dimension of mesoporous aluminosilicates to tens of nanometers makes the mesopore/macropore channel system in Au@MCM more accessible for CO oxidation, and the higher CO conversion could be obtained.[38] Moreover, we will show in another paper that MCM-41 can stabilize Au−Ag alloy particles through the interaction between defects associated with Al in MCM-41 and the Au−Ag alloy nanoparticles.[39] These defects can also facilitate O_2 adsorption on the Au−Ag alloy surface.

Conclusions

In summary, we have developed a novel one-pot synthesis procedure to prepare a highly active alloy catalyst, Au−Ag@MCM. In this method, although the preformed Au−Ag alloy nanoparticles in aqueous solution can be occluded successfully into mesoporous support with most of the alloy structure and particle size retained, the subsequent calcination process causes phase segregation and particle enlargement, which is induced by the formation of AgBr. Therefore, the reduction treatment is found to be necessary to remove the poisonous Br^- and the realloying of Au with Ag. The resultant Au−Ag alloy catalyst is very active for low-temperature CO oxidation by improving the adsorption and activation of oxygen.

Acknowledgment. This work was supported by a grant from the National Science Council through Academy Excellent program. We thank Professor C. Cheng and Dr. C. M. Wei for their help with theoretical modeling, Professor Tom Lin for the EPR experiment, and Mr. H. D. Wan for chemical analysis.

References and Notes

(1) Haruta, M.; Kobayashi, T.; Sano, H.; Yamada, N. *Chem. Lett.* **1987**, 405.

(2) Haruta, M. *Catal. Today* **1997**, *36*, 153.

(3) Bond, G. C.; Thompson D. T. *Catal. Rev.—Sci. Eng.* **1999**, *41*, 319.

(4) Carrettin, S.; Concepción, P.; Corma, A.; López Nieto, J. M.; Puntes, V. F. *Angew. Chem., Int. Ed.* **2004**, *43*, 2538.

(5) Daté, M.; Okumura, M.; Tsubota, S.; Haruta, M. *Angew. Chem., Int. Ed.* **2004**, *43*, 2129.

(6) Chen, M. S.; Goodman, D. W. *Science* **2004**, *306*, 252.

(7) Lopez, N.; Janssens, T. V. W.; Clausen, B. S.; Xu, Y.; Mavrikakis, M.; Bligaard, T.; Nørskov, J. K. *J. Catal.* **2004**, *223*, 232.

(8) Arrii, S.; Morfin, F.; Renouprez, A. J.; Rousset, J. L. *J. Am. Chem. Soc.* **2004**, *126*, 1199.

(9) Liu, Z. P.; Gong, X. Q.; Kohanoff, J.; Sanchez, C.; Hu, P. *Phys. Rev. Lett.* **2003**, *91*, 266102.

(10) Molina, L. M.; Hammer, B. *Phys. Rev. B* **2004**, *69*, 155424.

(11) Schubert, M. M.; Hackenberg, S.; van Veen, A. C.; Muhler, M.; Plazak, V.; Behm, R. J. *J. Catal.* **2001**, *197*, 113.

(12) Häkkinen, H.; Abbet, S.; Sanchez, A.; Heiz, U.; Landman, U. *Angew. Chem., Int. Ed.* **2003**, *42*, 1297.

(13) Venezia, A. M.; Liotta, L. F.; Pantaleo, G.; La Parola, V.; Deganello, G.; Beck, A.; Koppány, Zs.; Frey, K.; Horváth, D.; Guczi, L. *Appl. Catal., A* **2003**, *251*, 359.

(14) (a)Liu, J. H.; Wang, A. Q.; Lin, H. P.; Mou, C. Y. *J. Phys. Chem. B* **2005**, *109*, 40. (b) Wang, A. Q.; Liu, J. H.; Lin, S. D.; Lin, T. S.; Mou, C. Y. *J. Catal.* **2005**, *233*, 186.

(15) Boccuzzi, F.; Chiorino, A.; Manzoli, M.; Lu, P.; Akita, T.; Ichikawa, S.; Haruta, M. *J. Catal.* **2001**, *202*, 256.

(16) Choudhary, T. V.; Sivadinarayana, C.; Chusuei, C. C.; Datye, A. K.; Fackler, J. P., Jr.; Goodman, D. W. *J. Catal.* **2002**, *207*, 247.

(17) Kozlova, A. P.; Sugiyama, S.; Kozlov, A. I.; Asakura, K.; Iwasawa, Y. *J. Catal.* **1998**, *176*, 426.

(18) Kung, H. H.; Kung, M. C.; Costello, C. K. *J. Catal.* **2003**, *216*, 425.

(19) Lin, C. H.; Lin, S. D.; Lee, J. F. *Catal. Lett.* **2003**, *89*, 235.

(20) Costello, C. K.; Guzman, J.; Yang, J. H.; Wang, Y. M.; Kung, M. C.; Gates, B. C.; Kung, H. H. *J. Phys. Chem. B* **2004**, *108*, 12529.

(21) Iizuka, Y.; Kawamoto, A.; Akita, K.; Daté, M.; Tsubota, S.; Okumura, M.; Haruta, M. *Catal. Lett.* **2004**, *97*, 203.

(22) Ghosh, S. K.; Mandal, M.; Kundu, S.; Nath, S.; Pal, T. *Appl. Catal., A* **2004**, *268*, 61.

(23) Venezia, A. M.; Liotta, L. F.; Deganello, G.; Schay, Z.; Horváth, D.; Guczi, L. *Appl. Catal., A* **2001**, *211*, 167.

(24) Okumura, M.; Coronado, J. M.; Soria, J.; Haruta, M.; Conesa, J. C. *J. Catal.* **2001**, *203*, 168.

(25) Claus, P.; Brückner, A.; Mohr, C.; Hofmeister, *J. Am. Chem. Soc.* **2000**, *122*, 11430.

(26) Lin, H. P.; Chi, Y. S.; Lin, J. N.; Mou, C. Y.; Wan, B. Z. *Chem. Lett.* **2001**, *30*, 1116.

(27) (a) Hohenberg, P.; Kohn, W. *Phys. Rev.* **1964**, *136*, B864. (b) Kohn, W.; Sham, L. J. *Phys. Rev.* **1965**, *140*, A1133.

(28) (a) Kresse, G.; Hafner, J. *Phys. Rev. B* **1994**, *49*, 14251. (b) Kresse, G.; Furthmüller, J. *Comput. Mater. Sci.* **1996**, *6*, 15.

(29) (a) Blöchl, P. E. *Phys. Rev. B* **1994**, *50*, 17953. (b) Kresse, G.; Joubert, D. *Phys. Rev. B* **1999**, *59*, 1758.

(30) Perdew, J. P.; Burke, K.; Ernzerhof, M. *Phys. Rev. B* **1996**, *77*, 3865.

(31) Rodríguez-González, B.; Sánchez-Iglesias, A.; Giersig, M.; Liz-Marzán, L. M. *Faraday Discuss.* **2004**, *125*, 133.

(32) Mallin, M. P.; Murphy, C. J. *Nano Lett.* **2002**, *2*, 1235.

(33) Kondarides, D. I.; Verykios, X. E. *J. Catal.* **1996**, *158*, 363.

(34) Ag in the reduced catalyst was dissolved by concentrated nitric acid and ammonia sequentially. After filtration, the solution was acidified again with nitric acid. Extra silver nitrate solution was added to the filtered solution. No AgBr precipitate can be detected. A lower limit of the Br content was calculated from the solubility product of AgBr. This shows that the level of Br in the catalyst is below 1.1×10^{-11} mol/g catalyst. The hydrogen reduction step has practically removed all of the Br from the sample.

(35) Li, X.; Vannice, A. *J. Catal.* **1995**, *151*, 87.

(36) Sandell, A.; Bennich, P.; Nilsson, A.; Hernnäs, B.; Björneholm, O.; Mårtensson, N. *Surf. Sci.* **1994**, *310*, 16.

(37) Nakatsuji, H.; Hu, Z. M.; Nakai, H.; Ikeda, K. *Surf. Sci.* **1997**, *387*, 328.

(38) Liu, J. H.; Chi, Y. S.; Lin, H. P.; Mou, C. Y.; Wan, B. Z. *Catal. Today* **2004**, *93−95*, 141.

(39) Wang, A. Q.; Hsieh, Y. P.; Chen, Y. F.; Mou, C. Y. *J. Catal.* 2005, submitted for publication.